In situ generation and atomic scale imaging of slip traces with atomic force microscopy

Oele, W.F.; Kerssemakers, J.W J; de Hosson, J.T.M.

Published in:
Review of Scientific Instruments

DOI:
10.1063/1.1148419

Publication date:
1997

In situ generation and atomic scale imaging of slip traces with atomic force microscopy

W. F. Oele, J. W. J. Kerssemakers, and J. Th. M. De Hosson[a)]
Department of Applied Physics, Materials Science Centre, University of Groningen, Nijenborgh 4, 9747 AG Groningen, The Netherlands

(Received 21 July 1997; accepted for publication 9 September 1997)

We have designed, constructed, and tested a three-point bending system for *in situ* studies of slip in ionic crystals with an atomic force microscope (AFM). The work is aimed at developing a novel instrumental attachment for an *in situ* study of plastic deformation. The bending system is installed inside the optical head of the AFM on top of the piezoelectric scanner. Since the bending should not obstruct scanning, a piezocrystal is used for bending as well as an external stepper motor, which is connected with a screw in the bending system via a flexible shaft. The bending system performs over a relatively wide, continuous deflection range. The operation of the three-point bending system is illustrated by experiments on an ionic material in which the effect of macroscopic bending is demonstrated at an atomic scale. © *1997 American Institute of Physics.* [S0034-6748(97)02712-3]

I. INTRODUCTION

Detailed mechanical behavior of materials is of particular interest in various fields of materials science, because it may affect possible applications of engineering materials in constructions. For the investigation of the mechanical properties various tests are developed in which an external load is applied. Quite often a study of crack propagation and microstructure analysis of fracture surfaces are involved in such studies.[1–3] A frequently used experimental setup in the field of semibrittle materials is the so-called three-point bending setup. In such configuration, both *in situ* and postmortem observations of plastic deformation are performed, using various techniques such as scanning electron microscopy,[4] (SEM), scanning acoustic microscopy,[4] and scanning tunneling microscopy (STM).[5] In combination with such a three-point bending fixture, atomic force microscopy (AFM) has also be shown to be a suitable method for the *in situ* observation of crack propagation in semibrittle materials at a surface.[6] For imaging of even much smaller features such as atomic steps AFM possesses a great advantage over other high-resolution techniques, such as field ion microscopy and transmission electron microscopy, because no extensive sample preparation is required. Commonly in AFM the repulsive force between a tip mounted on a cantilever and a specimen is measured. Hence it is suitable to all kinds of materials, both electric conductors and insulators, i.e., in contrast to STM which can only be used for conducting and semiconducting materials. In this article a three-point bending system is combined with a commercial AFM, allowing for *in situ* slip trace generation and imaging. The working of the bending system is illustrated by experiments on an ionic material in which the effect of macroscopic bending is clearly demonstrated at an atomic scale.

II. INSTRUMENTATION

We have designed, constructed, and tested an *in situ* three-point bending system specifically for a Nanoscope II atomic force microscope from Digital Instruments. The work is aimed at introducing a novel tool, while keeping the usual application of this commercially available microscope unmodified: consequently, the bending system must be installed inside the optical head on top of the piezoelectric scanner. Moreover, bending should not obstruct scanning. This aim is achieved by using a piezocrystal for bending and an external stepper motor, which is connected with a screw in the bending system via a flexible shaft. The small space inside the optical head of the microscope restricts the dimensions of the three-point bending system. Figure 1 displays a schematic view of the experimental setup in which the microscope is not drawn as well as a schematic cross section of the bending system. As a consequence of the tiny dimensions, particular constraints are set on the properties of the materials for the three-point bending system. The material must be rigid so that the applied forces, which are required for bending, will plastically deform the specimens, but keep the housing intact. The maximum force until fracture of a specimen in a three-point bending configuration is determined by the modulus of rupture σ_{mr} and the Young's modulus E. For NaCl, which was used in this study, $\sigma_{\mathrm{mr}} = 3.9\ \mathrm{MPa}$[7] and $E = 3.65\times 10^4\ \mathrm{MPa}$.[8] Since the setup is cramped with space, the width and length of the sample should be smaller than 1.4 and 12 mm, respectively. Furthermore, to keep optimum maneuverability for the bending system as well as for the optical head, the height of the sample must lie in the range of 2.6–3.0 mm. With σ_{mr}, E and the dimensions of the sample, the maximum bending forces needed for the maximum deflection of a sample can be calculated. According to the pure bending theory, the range of the maximum force using the above parameters, is 0.5–2.0 N. The range of the accompanying deflection is 0.8–2.5 μm. A suitable material for the bending system is quartz (vitreous silica). Compared to NaCl, quartz is a rigid material. The Young's modulus of quartz is 7.22×10^4 MPa.[9] Because the applied bending forces needed for plastic deformation of the samples are relatively low, they will not break the housing even considering the brittle nature of quartz. We used HSQ 300 quartz from Heraeus, Germany. Quartz could be cut eas-

a)Author to whom correspondence should be addressed; Electronic mail: hossonj@phys.rug.nl

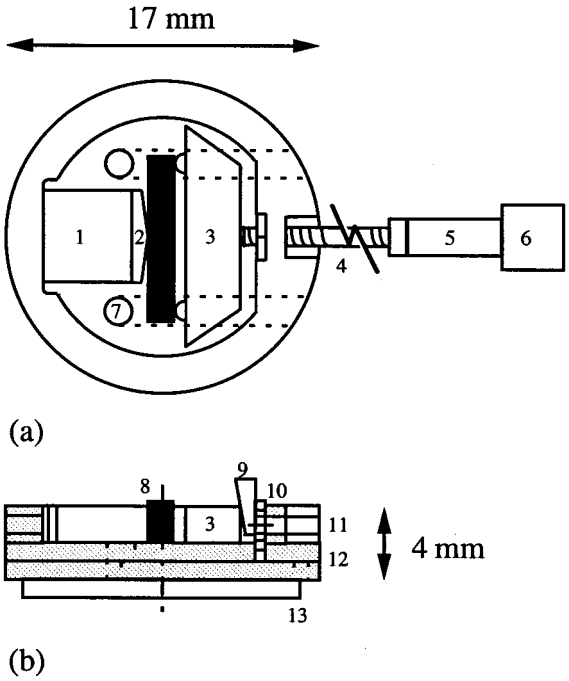

FIG. 1. Three-point bending system. (a) Schematic view of experimental setup; (b) cross section. (1) Modified PL-55.20 d^{33}-stack piezoelectric actuator element; (2) wedge; (3) double wedge; (4) screw; (5) heat shrink tubing; (6) KP4M4-023 stepper motor; (7) circular drain hole; (8) sample; (9) block wedge; (10) nut; (11) three layers O-ring shaped; (12) two closed shells; (13) metal layer.

ily with a continuous wave CO_2 laser. During cutting the power of the laser was 200 W and the laser scanning speed between 200–300 mm/min. As said before, it is essential that the housing is as rigid as possible. For this reason we implemented a quartz bottom plate in the design. However, the resulting cruciblelike shape of the bending system cannot be cut with the laser out of one piece. Therefore, the bending system must be composed of different, thin layers of quartz, which we glued together. The layered structure does not affect the rigidity, because the bending forces do not act in the direction of the glued contacts during bending. Moreover, due to cutting in thin layers, residual stresses from quartz cutting are small and annealing is not necessary. Using thin layers, the height of the bending system can also be kept as compact as possible. The three-point bending system is made of five layers that are glued together with an epoxy glue based on bisfenol A and epichlorhydrine. The glue has dried for 65 h at room temperature. The layers have a diameter of 17 mm, because for this diameter the 2×2 mm range of the xy table of the AFM microscope can be used completely. The first layer at the bottom is 1 mm thick and contains two slits for the wires of the piezocrystal. The second layer contains two circular holes through which the wires are led and a rectangular hole in which a brass nut has been sunk. Those two layers are closed shells. The next three layers are O rings. On the second layer the piezocrystal, the sample, and the double wedge lie. The third and fifth layer are identical and are used to gain the necessary depth for attaching the piezoelement against the sample holder. The fourth layer contains an aperture through which a brass screw is led. Be-

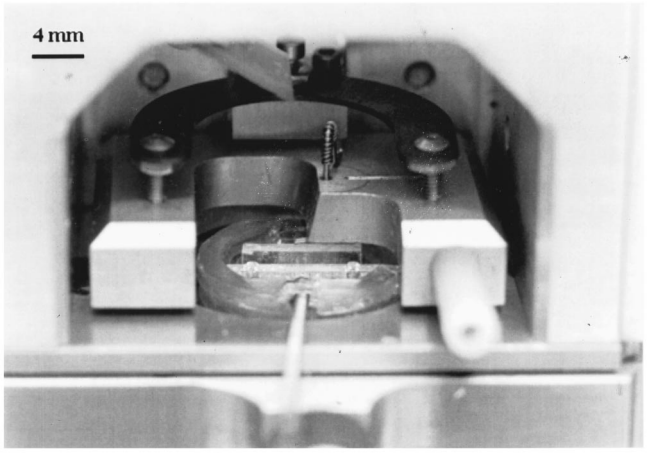

FIG. 2. Photograph of the experimental setup. The screw, element (4) in Fig. 1, is mounted above the xy table of the microscope.

cause we want to be able to tighten the screw during scanning, the screw must be externally accessible. Therefore, the screw must be mounted to the bending system above the xy table of the microscope as shown in Fig. 2. Together with the tip position and the demand that the screw must act in the middle of the double wedge, the height of the samples is determined and so the total height of the bending system. Using the sample dimensions as given before, this results in a total height of 4 mm. At the bottom a metal layer was mounted for attaching the three-point bending system to the magnetic top of the piezoelectric tube scanner. The wires of the piezo element in the sample holder are led under the optical head of the AFM to a power supply. The piezocrystal in the sample holder is a modified piezoelectric actuator element of Physik Instrumente GmbH & Co., Germany. The maximum expansion of the element at 100 V is 2.0 μm. The piezoelement is attached to the quartz rings with glue, so that during operation the expansion is oriented in the xy plane. On this piezoelement we glued a quartz wedge with a radius of 0.5 mm. The double wedge, also with a radius 0.5 mm, is made of quartz, as well. The bar can be pressed against the sample by the screw which is tightened by a stepper motor from Japan Servo Co., Ltd., Japan. We use the software of Nanoscope II to control the stepper motor. The minimum step that the stepper motor turns is 3.6°. The screw has a nominal 1 mm diameter with a lead of 0.25 mm (M1). As a result the forward movement of the screw with the smallest step of the stepper motor is 2.5 μm. Thus the piezoelement overlaps almost entirely the smallest step of the stepper motor allowing for fine tuning the applied bending force. In the experimental results shown in this article only the stepper motor was used because the force variation obtained with the piezoelement did not change the surface morphology. The flexible connection between the stepper motor and the screw is made of a heat shrink tubing from Multicomp with a length of 170 mm and a diameter of 2.4 mm. These parameters seemed to be suitable to satisfy the demands on the tubing during operation: The tubing has a relatively big torque resistance, while it is flexible in the xy plane. It also isolates the microscope acoustically from the stepper motor. These properties are important for tightening the screw dur-

ing scanning, because the sample holder must be able to move in the xy plane for AFM imaging. Simultaneously, the screw has to be able to be tightened far enough for the plastic deformation of the sample, while the vibrations of the stepper motor can influence the measurements. AFM imaging is acquired by maintaining a constant deflection signal using a feedback to the piezotube. The measurements were made with Si_3N_4 cantilevers with integrated tips from Nanoprobe (Digital Instruments). Extra attention is paid to the alignment of the bending forces that are obtained with the screw. The screw is not completely clamped in the nut and therefore the orientation of the screw and so the acting force can have an upward component and may cause buckling. If this buckling occurs, it can cause feedback instabilities. This disturbs the measurements because the surface climbs out of the range of the piezoelectric scanner and depending on the buckling motion the tip can be damaged. A downward component of the force is always obtained when the screw acts on a slant plane at the back of the double wedge. The double wedge will however be able to glide across the bottom plate. The use of a small block wedge, installed as shown in Fig. 1, also prevents the sample from an upward movement. Moreover, this prevents the sample from rotating around the wedge.

III. THEORETICAL CONCEPTS

Plastic deformation occurs when a crystal is sufficiently deformed beyond the elastic limit, the so-called yield stress, and at the same time the fracture stress lies above the yield stress. A bending load induces stresses in the crystal which, corresponding to plastic deformation, may respond by the movement of dislocations on specific slip planes. For dislocation movement across slip planes a characteristic shear stress is required.[10] The resolved shear stress is given by the product of applied stress and the Schmid factor:

$$\tau = \frac{F}{A} \cos\,\phi \cos\,\theta, \tag{1}$$

in which F is the applied force, $F\cos\theta$ is the force component in the slip direction, and this force acts over slip surface with area $A/\cos\phi$. Note ϕ is the angle between F and the normal to the slip plane. Dislocations moving out of the sample to the surface produce steps or slip lines. From classical studies utilizing etching techniques, the occurrence of so-called slip bands in plastically deformed NaCl is a well known fact.[11–14] These are regions of high slip density, parallel to the glide planes. In our setup, we image the bent substrate from the side, which means the scanned area covers a gradient in stress. To explain the character and distribution of single slip traces, a discussion on the stress distribution causing this slip is appropriate. The stress distribution applied by the three-point bending system is considered to fulfill the stress distribution as obtained from pure bending, in which a correction for the influence of the application of a concentrated load has to be made.

As will be shown, the magnitude of this so called wedge effect scales with the beam thickness. Therefore it should be taken into account in this study, because the possible scan area of the microscope is within 2 mm^2 of the wedge, compared to a beam thickness of $\sim$1.5 mm. Therefore, in this AFM setup we should not consider the wedge effect a small perturbation, but as a significant contribution to the stress present below the areas under investigation. According to the pure bending theory[15] the stress distribution in a rectangular beam is described by

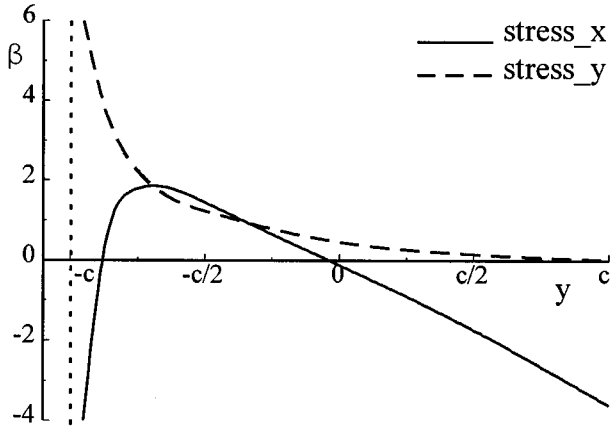

FIG. 3. Plot for a representative sample in which the numerical factor β for $(\sigma_y+\sigma_x')$ and σ_y as a function of the cross-sectional position is displayed, β being a measure for the applied stress. The positive values for β correspond to compressive stress. The constant c is half the width of the sample.

$$\sigma_x = \frac{3L}{8c^2}\left(1-2\left|\frac{x}{s}\right|\right) y\left(\frac{P}{c}\right), \tag{2}$$

in which P is the applied load force per wedge length, s the distance between the two wedges of the double wedge, and c is the half the width. Incorporating the wedge effect, it can be shown[16] that the stress σ_x can be split into two parts: one, which can be calculated by the usual elementary beam formula and an extra term, which represents the local effect near the point of application of the load. The second part, called σ_x', can be represented in the form $\beta(P/c)$, in which β is a numerical factor depending on the position of the point for which the local stresses are calculated. Due to the application of a concentrated load the stress components σ_y and τ_{xy} will be no longer zero and they can also be represented in the form $\beta(P/c)$. The local stresses decrease rapidly with increase of the distance from the point of application of the load and at a distance equal to the depth of the beam the local stresses are usual negligibly small. In Fig. 3 a schematic picture is presented in which the complete uniaxial stress $(\sigma_x+\sigma_x')$ expressed in the numerical factor β is plotted as a function of the position across the cross section of a bar of representative dimensions.

IV. PERFORMANCE

Although no extensive sample preparation is needed in AFM, the sample surface must be flat, smooth and must have a low density of steps. Otherwise, the shape of the probe tip may influence the measurements of the surface profile. In this study we tested the designed bending system on NaCl monocrystals from Korth-Kristall, Germany to illustrate the working of the bending system. The required surface is easily prepared from NaCl monocrystals by cleaving across the

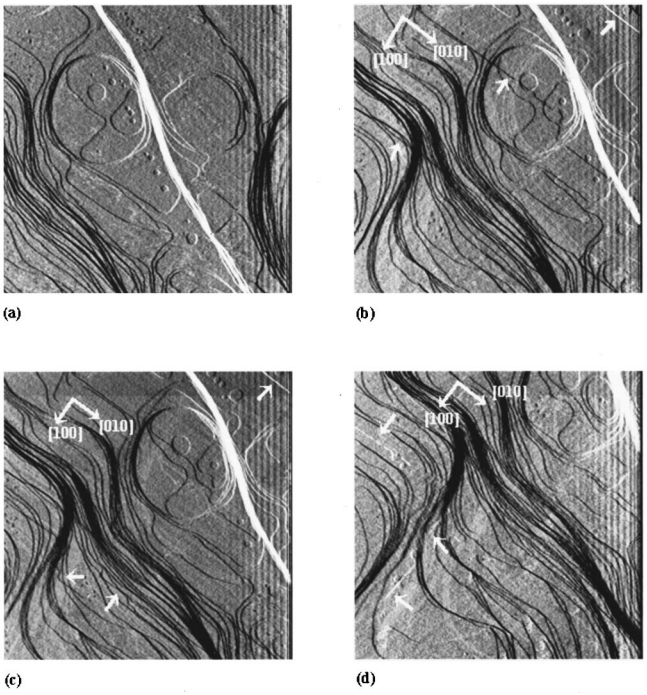

FIG. 4. $5.9\times5.9\ \mu m^2$ AFM images of the same area of an *in situ* bent NaCl [100] monocrystal. Variations in position stem from the clamping routine. The large circular island in the center may serve as a guide for the eye. (a) AFM image of an area, still in elastic range. The flowing, smooth atomic steps are characteristic for freshly cleaved NaCl [100] surfaces. (b) Image of the same area, with introduction of slip traces indicated by markers. The sign of the slip traces indicates that the compression in this region is relieved by (011)[011] glide (white trace) as well as (011)[011] glide (black traces). (c) After further increase of the applied bending load, some more straight ledges are introduced. Comparing the trace indicated by the lowest marker with its shorter precursor in 4(b), left-most marker, we observe that a cross slip along [010] and [100] traces has occurred. (d) Last image before fracture, with a new cross slipped trace on [010] and [100] glide planes but of opposite sign to the one emerging in 4(c).

{100} planes, the cleaving planes of NaCl.[17] The cleaved samples are placed in the bending system as shown in Fig. 1. An example of newly emerging slip traces is shown in Fig. 4, where approximately the same area was imaged during successive increments of bending of a $9.55\times2.85\times1.05$ mm sample. The distance s between the knife edges of the double wedge is 8 mm. After each stepper motor increment the corresponding translation of the surface is manually readjusted, leaving small variations in the position of the scanned area. The large circular island in the center serves as a guide for the eye. In the present setup, no information on force or bending amplitude can yet be obtained. The images were taken 100–200 μm from the wedge and so being on the compressive part of the sample. Between each image an increment of bending was applied. Image 4(a) shows a characteristic scan of a cleaved NaCl surface. It contains islands, cusps, grains, and smooth ledges known from previous studies.[18–20] The sample is clamped in the bending system, but still in the elastic range. This can be concluded from comparing this scan with previous scans (not displayed) in which the applied bending deflection was significantly smaller. The scans did not show any differences. Image 4(b) is the first image displaying surface changes. Some new, straight slip traces are introduced, indicated by the upper two

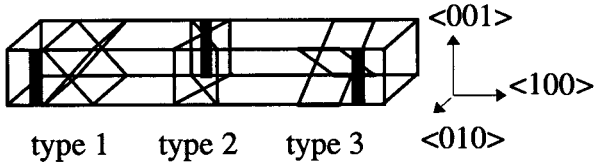

FIG. 5. Sketch of sample with {110}⟨110⟩ slip system. Slip planes are subdivided in three sets of orthogonal slip planes named type 1, 2, and 3.

small markers. Obviously, the applied stress in the crystal is now bigger than the yield stress and dislocation movement is taking place. As explained in Sec. III about the theoretical concepts, the applied bending load causes stresses in the crystal which can activate specific slip planes depending on the Schmid factor. The primary slip system in [100]-oriented NaCl monocrystals is the {110}⟨110⟩ slip system.[17] The slip planes occur in three sets of orthogonal slip planes named type 1, 2, and 3 (see Fig. 5). When those slip planes are activated, the sets of type 1 and 3 become visible at the scanning surface as a straight ledge oriented in the [010] and [100] directions, respectively. This explains that the traces are oriented in the [010] direction. The crystallographic orientation was deduced from the angle between the scan direction of the tip and the direction of the [100]-oriented monocrystal in the bending system. The sign of the slip traces indicates that the compression in this region is relieved by (011)[011] glide (white trace) as well as (011)[011] glide (black traces). After further increase of the applied bending load, some more straight ledges are introduced as can be seen in image 4(c). Comparing the trace indicated by the lowest marker with its shorter precursor in 4(b), left-most marker, we observe that a cross slip along [010] and [100] traces has occurred, similar to those observed by means of gold decoration techniques by Appel *et al.*[19] As these slip planes do not share a component of Burger's vector of any edge, this implies a dislocation node, some climb process, or screw dislocation movement.[19] Image 4(d) shows the last image before fracture, with a new cross slipped trace on [010] and [100] glide planes but of opposite sign to the one emerging in 4(c).

The set of type 2 cannot be detected at this surface. Due to the Schmid factor the set of slip planes of type 1 and 3 can only be activated by the stress $(\sigma_x+\sigma_x')$ and the stress $(\sigma_y+\tau_{xy})$, respectively. According to the Seewald correction for the stress distribution in three-point bending the stress $(\sigma_y+\tau_{xy})$ is solely introduced by the wedge effect. As can be concluded from Fig. 5, if slip traces of type 3 planes are observed, the Seewald correction must be involved in the description of the stress distribution. This is confirmed by Fig. 6. This figure is the first $8.8\times8.8\ \mu m^2$ scan of a subsequent series of eight scans across the cross section of a bent sample of dimensions $9.10\times2.85\times1.40$ mm. The scan series is located at a region in the compressive part about 250 μm from the wedge towards the center of the sample. Note that all slip traces bear the same sign, indicating a slip bandlike behavior for both types. This implies only one glide plane per type is involved in this compression region. However the actual number of individual slip traces observed is low and

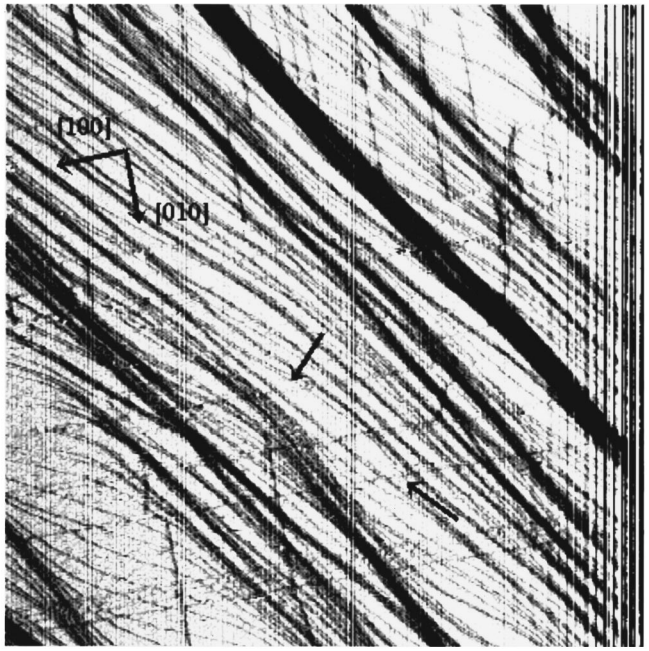

FIG. 6. $8.8\times8.8\ \mu m^2$ AFM image of a high slip trace concentration. The flowing, smooth atomic steps are characteristic for freshly cleaved NaCl [100] surfaces. Introduced straight ledges are oriented in the [010] and [100] direction. Some straight ledges are indicated by markers. The straight ledges cross the smooth ledges, demonstrating that the straight ledges are a consequence of slip.

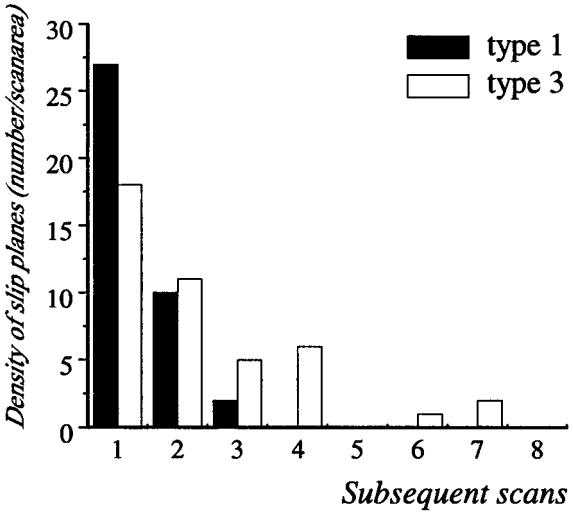

FIG. 7. Histogram of the density of slip planes per scan image of area $7.7\times10^{-11}\ m^2$ for eight subsequent AFM images. The horizontal axis spans a range of $\sim50\ \mu m$, measured at approximately $-c/2$ in Fig. 3. For this specific sample, this corresponds to $\sim250\ \mu m$.

rather widely spaced on an atomic scale, making the slip band character still rather weak.

A slip trace count was performed from this series of eight scans. In Fig. 7 the resulting densities of visible slip planes of type 1 and 3, respectively, are plotted as a function of each scan. Scans much closer to the wedge (not displayed) yield a much higher density of slip lines, which confirms that this trend in distribution extends over rather long distances. The counts of both types should be interpreted differently: a decrease of one count of [010] traces from scan to scan, means a slip trace has stopped there at a screw-character point. On the other hand each count of the [100] traces expresses a different slip line.

By correlating the number of mobile dislocations on {110} slip planes to the applied stress in the sample we observe that the density of slip planes in this part of the sample decreases as predicted from Fig. 3. However, we should be cautious in linking the observed distribution very strongly to the stress distribution, as the generation process of dislocations corresponding to the emerged slip traces is unknown. A close match of slip trace density with stress distribution is only appropriate if there is a one-to-one relation of slip traces with an original homogeneous bulk distribution of dislocations. However, this may not be the case. Slip bands are well known in NaCl deformation experiments,[11–14,19] where for instance, multiple cross glide and annihilation cause large deviations of the number of observed slip lines with that of the original dislocation density. Moreover, large numbers of dislocations could be generated and sent into the substrate at the wedge line at $-c$, where stress is highest (see Fig. 3). However, because the number of [100] slip traces decreases in an analogous manner as the cutting off of the [010] slip traces, we believe the gradient of counts along the $\langle010\rangle$ direction still reflects the stress distribution. This is because the more slip traces per area are counted, the more the local yield should have been, independent of the origin of emerged dislocations.

The presented images show also other features as interactions of the introduced straight ledges with the existing smooth ledges known from Appel *et al.*,[19] but this is beyond the scope of this study. The concept of the applied stress distribution in a bent sample and the resulting activation of specific slip planes is confirmed by measurements in which we compressed [100]-oriented samples in the [100] direction. After compressing, only one type of slip planes is detected on a surface with AFM as expected from the Schmid factor. Therefore, from the activation of specific slip planes in [100]-directed NaCl monocrystals it can be concluded that we have constructed a three-point bending system in which the applied stress distribution can be described taking the Seewald correction into account for three-point bending. The applied stress distribution seems well reflected by the surface features as observed by AFM and this bending system is suitable for experiments on other types of materials.

[1] R. M. Thomson, Solid State Phys. **39**, 1 (1986).
[2] H. Koizumi and T. Suzuki, Phys. Status Solidi A **68**, 579 (1981).
[3] P. Wang and C. Ruiz, Mater. Sci. Eng. A **127**, 105 (1990).
[4] A. Kohyama, N. Niwa, and S. Sato, Key Eng. Mater. **79**, 279 (1993).
[5] Th. Fries, K. Oster, and K. Wandelt, Acta Metall. Mater. **42**, 3129 (1994).
[6] M. Göken, H. Vehoff, and P. Neumann, J. Vac. Sci. Technol. B **14**, 1157 (1996).
[7] L. S. Combes, S. S. Ballard, and K. A. McCarthy, *Gmelins Handbuch der Anorganischen Chemie* (Springer, Berlin, 1972).
[8] S. V. Subrahmanyam, in Ref. 7.
[9] J. M. Ide, *Gmelins Handbuch der Anorganischen Chemie* (Springer, Berlin, 1959).
[10] D. Hull and D. J. Bacon, *Introduction to Dislocations* (Pergamon, Oxford, 1984).
[11] R. W. Davidge and P. L. Pratt, Phys. Status Solidi **6**, 759 (1964).
[12] G. Kästner, Phys. Status Solidi **36**, 261 (1969).

[13] A. S. Argon, A. K. Nigam, and G. E. Padawer, Philos. Mag. **25**, 1095 (1972).
[14] T. Hagihara, J. Phys. Soc. Jpn. **41**, 857 (1976).
[15] S. Timoshenko, *Strength of Materials*, edited by F. R. Shanley (McGraw-Hill, New York, 1957).
[16] S. Timoshenko and J. N. Goodier, *Theory of Elasticity* (McGraw-Hill, New York, 1951).
[17] S. Amelinckx, *Dislocations in Solids*, edited by F. R. N. Nabarro (North Holland, Amsterdam, 1982).
[18] H. Bethge, Phys. Status Solidi **2**, 775 (1962).
[19] F. Appel, U. Messerschmidt, and V. Schmidt, Mater Sci. Eng. **56**, 211 (1982).
[20] E. Meyer, R. Lüthi, L. Howald, M. Bammerlin, M. Guggisberg, and H.-J. Güntherodt, J. Vac. Sci. Technol. B **14**, 1285 (1996).